The Photochemistry of Ethylene Episulfoxide

Fei Wu, Xirong Chen, and Brad R. Weiner*

Contribution from the Department of Chemistry and Chemical Physics Program, University of Puerto Rico, Box 23346 UPR Station, Río Piedras, Puerto Rico 00931

Received March 25, 1996[⊗]

Abstract: The photochemistry of ethylene episulfoxide, C_2H_4SO, has been investigated for the first time by using time-resolved laser-induced fluorescence (LIF) spectroscopy to probe the $SO(X^3\Sigma^-)$ photofragment on the ($B^3\Sigma^- - X^3\Sigma^-$) transition. Photodissociation of C_2H_4SO at 193 and 248 nm produces $SO(v'' = 0-6)$ and $SO(v'' = 0-5)$, respectively. The vibrational state distributions of the SO photofragment are inverted with maxima at $v'' = 1$ in both cases. Franck−Condon and impulsive models have been used to fit the experimentally observed vibrational state distributions and the internal energy content of the nascent $SO(X^3\Sigma^-)$ photofragment. These models are unable to fit the experimental observations, when the other fragment is ground-state ethylene, but excellent agreement is obtained for the lowest energy triplet state of C_2H_4. The time-dependent behavior of the $SO(X^3\Sigma^-)$ LIF signal has been measured, indicating a second ground-state sulfur monoxide production pathway. The experimental $SO(X^3\Sigma^-)$ transients can be fit by a biexponential function. The slower production of $SO(X^3\Sigma^-)$ is believed to be due to relaxation of $SO(a^1\Delta)$, which is also produced in the photodissociation of C_2H_4SO. Quantum yields for the production of $SO(X^3\Sigma^-)$ and $SO(a^1\Delta)$, based on a kinetic analysis, are 0.25 ± 0.04 and 0.41 ± 0.06 following 193 nm irradiation of C_2H_4SO and 0.34 ± 0.06 and 0.44 ± 0.08 for the 248 nm photolysis.

1. Introduction

Resolution of the energy disposal into the nascent products of a chemical reaction provides information on the transition state structure and interactions between the separating fragments in the exit channel. A large body of work, both experimental and theoretical on unimolecular fragmentation reactions corroborates this assertion and suggests that photodissociation dynamics studies may be the primary method for obtaining information about the excited states of polyatomic molecules.[1] The advantages of these photochemical excitation methods can be fully realized only if the interrelationships between potential energy surface topology, photophysical processes, and chemical pathways are unambiguously characterized.

The photodissociation as well as the thermal decomposition of homocyclic and heterocyclic ring compounds have been studied by several groups in recent years.[2−4] In many of these studies, efforts have been focused on elucidating whether the thermal decomposition and/or photodissociation of these prototypical carbonyl and azo compounds proceed via a concerted or a stepwise multiple bond cleavage process, by measuring the energy disposal into the CO and N_2 products, respectively. In particular, the extensive studies of the photodissociation dynamics of cyclic ketones have contributed to a much greater understanding of the unimolecular reaction chemistry of these ring compounds as well as to the flow of energy to the products during the fragmentation process.[3] The same level of scrutiny has not been broadly applied to the heterocyclic ring compounds.

The photodissociation of the simplest sulfur-containing organic ring compound, ethylene sulfide (thiirane) has been studied in two groups.[5,6] Bersohn and co-workers have investigated the 193 nm photodissociation dynamics of ethylene sulfide at 193 nm by monitoring the state specific production of atomic sulfur with high resolution laser spectroscopy. They concluded that the dissociation is direct and symmetric, *i.e.*, both C−S bonds break simultaneously to produce C_2H_4 and $S(^1D)$.[5] Felder *et al*. have studied the 193 nm photodissociation of thiirane by using a time-of-flight crossed laser-molecular beam technique.[6] They identified three primary dissociation channels, *i.e.*, a dominant (80%) hydrogen abstraction channel to produce $H + SC_2H_3$ and two minor (∼10% each) dissociation channels, which form $S + C_2H_4$ and $HS + C_2H_3$. The observed sulfur atom production channel confirms the experiments of Bersohn and co-workers and is consistent with their electronic state determination. The photochemistry of cyclic sulfoxides in the gas phase has received limited attention. Dorer and Salomon measured the stable hydrocarbon products by gas chromatography/mass spectrometry methods following the ultraviolet flash photolysis of trimethylene sulfoxide (TRSO) and tetramethylene sulfoxide (TMSO).[7] In both cases, they

* To whom correspondence should be addressed.

⊗ Abstract published in *Advance ACS Abstracts,* August 1, 1996.

(1) See for example, *Molecular Photodissociation Dynamics*; Ashfold, M. N. R., Baggott, J. E.; Eds.; Royal Society of Chemistry: London, 1977. Schinke, R. *Photodissociation Dynamics*; Cambridge University Press: Cambridge, 1993.

(2) (a). Adam, W.; Wang, G. *J. Org. Chem.* **1991**, *56*, 3315. (b). Adam, W.; De Lucchi, O.; Dörr, M. *J. Am. Chem. Soc.* **1989**, *111*, 5209. (c). Adam, W.; OppenlÑnder, T.; Zang, G. *J. Org. Chem.* **1985**, *50*, 3303. (d). Adam, W.; Gillaspey, W. D.; Peters, E.-M.; Peters, K.; Rosenthal, R. J.; von Schnering, H. G. *J. Org. Chem.* **1985**, *50*, 580−595. (e) Adam, W.; Carballeira, N.; Gillaspey, W. D. *Tetrahedron Lett.* **1983**, *24*, 5473. (f) Chang, M. H.; Jain, R.; Dougherty, D. A. *J. Am. Chem. Soc.* **1984**, *106*, 4211. (g) Simpson, C. J. S. M.; Wilson, G. J.; Adam, W. *J. Am. Chem. Soc.* **1991**, *113*, 4728. (h) Buxton, J. P.; Simpson, C. J. S. M. *Chem. Phys.* **1986**, *105*, 307. (i) Simpson, C. J. S. M.; Price, J.; Holmes, G.; Adam, W.; Martin, H.-D.; Bish, S. *J. Am. Chem. Soc.* **1990**, *112*, 5089. (j) Dolbler, W. R.; Frey, H. M. *J. Chem. Soc., Perkin Trans.* **1974**, *2*, 1647. (k) Hess, L. D.; Pitts, J. N. *J. Am. Chem. Soc.* **1984**, *106*, 4211.

(3) (a) Jimenez, R.; Kable, H. S.; Loison, J-C.; Simpson, C. J. S. M.; Adam, W.; Houston, P. L. *J. Phys. Chem.* **1992**, *96*, 4188. (b). Trentelman, K. A.; Moss, D. B.; Kable, S. H.; Houston, P. L. *J. Phys. Chem.* **1990**, *94*, 3031. (c) Sonobe, B. I.; Fletcher, T. R.; Rosenfeld, R. N. *J. Am. Chem. Soc.* **1984**, *106*, 4352−4356, 5800−5805. (d) Sonobe, B. I.; Fletcher, T. R.; Rosenfeld, R. N. *Chem. Phys. Lett.* **1984**, *105*, 322, (e) Prather, R. A.; Rosenfeld, R. N. *J. Phys. Chem.* **1991**, *95*, 6544.

(4) Adam, J. S.; Engel, P. S.; Weisman, R. B. *J. Am. Chem. Soc.* **1990**, *112*, 9115.

(5) Kim, H. L.; Satyapal, S.; Brewer, P.; Bersohn, R. *J. Chem. Phys.* **1989**, *91*, 1047.

(6) Felder, P.; Wannemacher, E. A. J.; Wiedmer, I.; Huber, J. R. *J. Chem. Phys.* **1992**, *96*, 4470.

(7) Dorer, F. H.; Salomon, K. E. *J. Phys. Chem.* **1980**, *84*, 1302.

S0002-7863(96)00968-7 CCC: $12.00

proposed a sulfinyl diradical intermediate to account for their observations. Pump-probe studies in our laboratory have measured the nascent vibrational energy distributions of the $SO(X^3\Sigma^-)$ photofragment following 193 and 248 nm photolysis of TRSO and TMSO as well as ethylene episulfoxide.[8,9] Our results are in excellent agreement with Dorer and Salomon for the TMSO photodissociation but disagree with their mechanism for the TRSO photolysis.

Ethylene episulfoxide (C_2H_4SO) has been employed as a pyrolytic source of SO radicals.[10] The thermal decomposition has also been studied theoretically as a compelling model of the three-membered heterocyclic ring system.[11,12] Pyrolysis of C_2H_4SO produces ethylene and sulfur monoxide, with the SO only detected in the ground state by Saito, using microwave spectroscopy,[13] and by Nishitani *et al.*, employing vacuum ultraviolet photoionization spectroscopy.[14] In a recent study, Gross *et al.* decomposed C_2H_4SO with a pulsed CO_2 laser and monitored the nature and evolution of the products by time-resolved FTIR spectroscopy. They found that the products produced under collision-free conditions are almost exclusively ethylene and $SO(X^3\Sigma^-)$.[15] There are no reports of any study of the UV photodissociation of ethylene episulfoxide in the literature. The photolysis of C_2H_4SO is a possible source of $SO(a^1\Delta)$, which lies *ca.* 18 kcal/mol above the ground state[16] and can be generated via a spin-allowed reaction.

We report here our detailed investigation of the ultraviolet photodissociation of ethylene episulfoxide, studied by probing the nascent $SO(X^3\Sigma^-)$ photofragment of C_2H_4SO using laser induced fluorescence (LIF) spectroscopy on the $(B^3\Sigma^- - X^3\Sigma^-)$ transition.

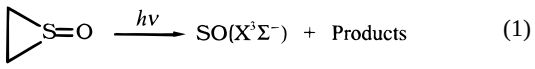

(1)

Laser induced fluorescence (LIF) spectroscopy of the SO-(B-X) transition has been shown previously to be an excellent method for measuring ground-state sulfur monoxide vibrational state distributions.[8,17] The real time behavior of the $SO(X^3\Sigma^-)$ photofragment is monitored to determine the participation of higher electronic states of sulfur monoxide as direct photoproducts. The relative vibrational state distributions as well as the quantum yields of the nascent $SO(X^3\Sigma^-)$ photofragment following 193 and 248 nm photolysis, are reported. The quantum yields of the nascent sulfur monoxide photofragment produced in higher excited states, following 193 and 248 nm photolyses have also been determined by analyzing the time behavior of the $SO(X^3\Sigma^-)$ photofragment. The resultant nascent vibrational energy distributions are fit to physical models to help determine the viable photodissociation mechanisms.

2. Experimental Section

Our experimental approach employs a typical two laser pump-probe system which has been described previously.[18] Ethylene episulfoxide is stored neat in a glass trap, from which it is expanded to a partial pressure of 5−20 mTorr into a stainless steel reaction chamber. The reaction chamber is equipped with extension arms (with baffles inside to reduce scattered light) and fused SiO_2 windows. Helium buffer gas (200−300 mTorr) is flowed across the reaction chamber windows to minimize the build up of heterogeneous photolysis products. All partial and total pressures are measured at the exit of the chamber by calibrated capacitance manometers.

Ethylene episulfoxide is photolyzed by an excimer laser (Lambda Physik LPX205), operating at either 193 nm (6−12 mJ/cm^2) or 248 nm (30−50 mJ/cm^2). The SO photofragments are monitored by LIF on the (B-X) transition in the 237−300 nm region of the spectrum. The probe laser light is generated by frequency doubling (β-BaB_2O_4) the output of a Lambda Physik LPD3002 tunable dye laser, which is pumped by a Lambda Physik LPX205 excimer laser operating on the XeCl transition at 308 nm. Three dyes, coumarin 480, 503, and 540A, are used in order to cover the entire frequency region of the SO signal. The two laser beams, photolysis and probe, are collinearly counter-propagated along the length of the cell to maximize overlap in the center of the reaction chamber.

Fluorescence is viewed at 90° relative to the laser beam axis by a high gain photomultiplier tube (PMT) through two long-pass filters and a band pass filter. The output of the PMT is signal-averaged by a gated integrator and sent to a microcomputer for display, storage, and analysis. The delay time between photolysis and probe lasers is controlled by a programmable delay generator. For a fixed delay time between photolysis and probe laser, the frequency-doubled output of the dye laser is scanned while collecting the total fluorescence signal to obtain a nascent LIF excitation spectrum. Data were collected at 30 Hz, with each point representing the average of 10 shots. The LIF intensity is found to be a linear function of the dye laser power, and signals taken over a large wavelength region were normalized to the dye laser power. For photolysis of ethylene episulfoxide at either 193 or 248 nm, a linear dependence on pump laser fluence was observed, indicating that the ground-state SO is produced by a single photon process in all cases. Temporal profiles of the $SO(X^3\Sigma^-)$ were obtained by scanning the delay (0−300 μs) time between the pump and probe lasers.

Ethylene episulfoxide was prepared by the oxidation of ethylene sulfide (Aldrich) according to the method of Kondo and Negishi.[19] The purified compound was identified by NMR analyses[20] and was subjected to three freeze−pump−thaw cycles prior to use. Sulfur dioxide and helium (Air Products, 99.9%) were used without further purification as a calibrant and a buffer gas, respectively, in the quantum yield measurements.

The vapor pressure of ethylene episulfoxide at room temperature was measured by a calibrated capacitance manometer in a glass vacuum system. The UV absorption spectrum was measured by using a HP 8452A diode-array spectrophotometer at room temperature.

3. Results

3.1. Direct Photolytic Production of $SO(X^3\Sigma^-)$. LIF signals, assignable to the $SO(B^3\Sigma^-, v' = 1 - X^3\Sigma^- v'' = 1)$ transition, have been recorded under collision-free conditions, where the total pressure in the reaction chamber is 200 mTorr, and the probe delay time is less than 100 ns. To avoid the interference of the emission induced by the photolysis laser, LIF spectra were recorded at longer probe delay times (*i.e.*, 1 μs). Under these conditions, *ca.* 2 gas kinetic collisions, relaxation of the nascent vibrational state distribution of the SO photofragment is negligible, while the rotational state populations are partially relaxed.[17b] The relative vibrational state populations of $SO(X^3\Sigma^-)$, N_V, were obtained by integrating the

(8) Wu, F.; Chen, X.; Weiner, B. R. *J. Phys. Chem.* **1995**, *99*, 17380.
(9) Wu, F.; Chen, X.; Weiner, B. R. SPIE-Proceedings **1995**, *2548*, 355.
(10) Salama, F.; Frei, H. *J. Phys. Chem.* **1989**, *93*, 1285−1292
(11) Hargittai, I. *The Structure of Volatile Sulphur Compounds*; D. Reidel Publishing Company: Dordrech/Boston/Lancaster, 1985.
(12) (a) Rohmer M.-M.; Roos, B. *J. Am. Chem. Soc.* **1975**, *97*, 2025. (b) Maccagnani, G.; Schlegel, H. B.; Tonachini, G. *J. Org. Chem.* **1987**, *52*, 4961.
(13) Saito, S. *Bull. Chem. Soc. Jpn.* **1969**, *42*, 667.
(14) Nishitani, E.; Fukuda, K.; Tanaka, I. *Bull. Chem. Soc. Jpn.* **1985**, *58*, 3475.
(15) Gross, H.; He, Y.; Quack, M.; Schmid, A.; Seyfang, G. *Chem. Phys. Lett.* **1993**, *213*, 122.
(16) Barnes, I.; Becker, K. H.; Fink, E. H. *Chem. Phys. Lett.* **1079**, *67*, 310.
(17) (a) Wang, H.; Chen, X.; Weiner, B. R. *Chem. Phys. Lett.* **1993**, *216*, 537. (b) Wang, H.; Chen, X.; Weiner, B. R. *J. Phys. Chem.* **1993**, *97*, 12260. (c) Chen, X.; Wang, H.; Weiner, B. R.; Hawley, M.; Nelson, H. H. *J. Phys. Chem.* **1993**, *97*, 12269.
(18) Barnhard, K. I.; Santiago, A.; He, M.; Asmar F.; Weiner, B. R. *Chem. Phys. Lett.* **1991**, *178*, 150.
(19) Kondo, K.; Negishi, A. *Tetrahedron* **1971**, *27*, 4831.
(20) Rasheed, K.; Warkentin, J. D. *J. Org. Chem.* **1980**, *45*, 4807.

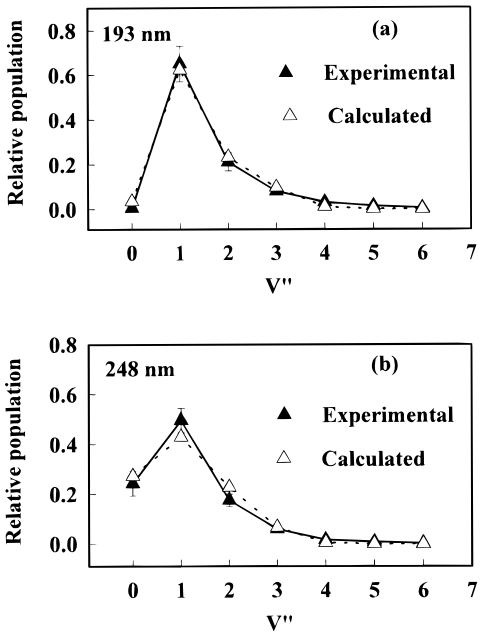

Figure 1. Experimental (▲) and calculated (△) vibrational state distributions of the nascent SO($X^3\Sigma^-$) photofragment following (a) 193 nm and (b) 248 nm photolysis of ethylene episulfoxide.

areas under the (1,v'') vibronic transitions (where $v'' = 0-6$) and correcting the integrated areas by the appropriate Franck−Condon factor.[21] The experimental vibrational distributions of the nascent SO($X^3\Sigma^-$) photofragment following irradiation of C_2H_4SO at 193 and 248 nm are found to be inverted with maximum population at $v'' = 1$, as shown in Figure 1.

We have measured the rotational state distributions of the ground-state SO radical in the $v'' = 1-4$ vibrational levels, following C_2H_4SO photolysis at both wavelengths. Rotational state distributions for the $v'' = 0$, 5, and 6 vibrational levels have not been measured, due to the low signal-to-noise ratio. The relative rotational state populations are determined by measuring the intensity of each well-resolved rovibronic transition, dividing by the appropriate line strength, *i.e.*, Hönl-London factor,[22] and multiplying by the corresponding rotational degeneracy. Typical Boltzmann plots, *i.e.*, ln(population/degeneracy) vs rotational energy, are shown in Figure 2. All the measured rotational state distributions can be reasonably described by a temperature. The rotational temperatures of the nascent SO photofragment are shown in Table 1.

We have also measured the quantum yields of SO($X^3\Sigma^-$) production at both photolysis wavelengths, which may provide insight into the photodissociation mechanism of ethylene episulfoxide. In our experiments, the LIF signal of a given rovibronic transition, corresponding to SO($X^3\Sigma^-$,$v'' = 1$, $N'' = 13$) vibrational state was used to measure the quantum yield. We recorded the LIF signal intensities originating from SO($X^3\Sigma^-$) following the photodissociation of C_2H_4SO and SO_2, respectively, under identical conditions except for the photolysis laser fluence (9.4 mJ/cm^2 at 193 nm and 57 mJ/cm^2 at 248 nm). The relative SO($X^3\Sigma^-$) quantum yield, ϕ, was derived as follows

$$\phi = I_{SO}/(\sigma \cdot P(v'') \cdot P_{laser}) \qquad (2)$$

where I_{SO} is the intensity of SO(B − X) signal, σ is the absorption cross section of the parent molecule at the corresponding photolysis wavelength, $P(v'')$ is the fractional nascent population in the vibrational state of SO($X^3\Sigma^-$, $v'' = 2$), and P_{laser} is the fluence of the photolysis laser. The vapor pressure of C_2H_4SO at room temperature is found to be 680 ± 40 mTorr. The UV absorption spectrum is structureless with an onset around 250 nm. From those measurements, the absorption cross sections are found to be $\sigma_{193} = (7.7 \pm 0.5) \times 10^{-18}$ cm^2 molecule^{-1} and $\sigma_{248} = (1.8 \pm 0.2) \times 10^{-19}$ cm^2 molecule^{-1} These cross sections are used to calculate the quantum yields of SO($X^3\Sigma^-$) from the 193 and 248 nm photolyses of C_2H_4SO. Since the SO($X^3\Sigma^-$) production yield is greater then 99.5% from the 193 nm photolysis of SO_2,[23] we assume it to be unity. By comparing ϕ from the photolysis of C_2H_4SO at both 193 and 248 nm with the ϕ value from the photolysis of SO_2 at 193 nm, the absolute quantum yield, Φ, of SO($X^3\Sigma^-$) from C_2H_4SO was obtained

$$\Phi_{SO}^{193} = \Phi_{193nm}^{TMSO}/\Phi_{193nm}^{SO2} = 0.25 \pm 0.04$$

$$\Phi_{SO}^{248} = \Phi_{248nm}^{TMSO}/\Phi_{193nm}^{SO2} = 0.34 \pm 0.06$$

The errors were obtained on statistical analysis (2σ).

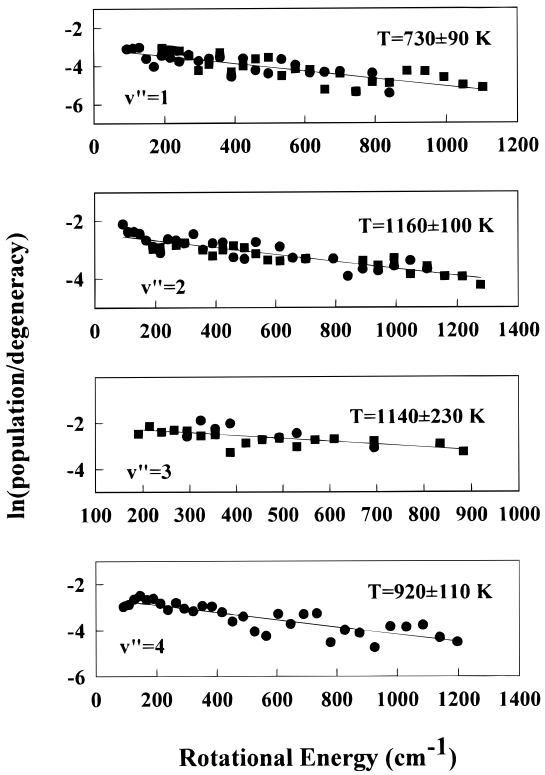

Figure 2. Boltzmann plots of the nascent rotational state distributions of SO($X^3\Sigma^-$,$v'' = 1-4$) resulting from the 193 nm photolysis of ethylene episulfoxide and linear least square fits to the data. The temperatures are obtained from the slopes of best fit lines, and the errors are statistical (1σ). The symbols ● and ■ are the P_{22} and R_{22} branch of SO($B^3\Sigma^-$, v' − $X^3\Sigma^-$, v'') transitions, respectively.

Table 1. Rotational Temperatures of the Photolytically Produced SO ($X^3\Sigma^-$) Fragment

photolysis wavelength (nm)	$v'' = 1$	$v'' = 2$	$v'' = 3$	$v'' = 4$
193	730 ± 90 K	1160 ± 100 K	1140 ± 230 K	920 ±110 K
248	640 ± 80 K	920 ± 70 K	1010 ± 160 K	970 ± 70 K

(21) Smith, W. H.; Liszt, H. S. *J. Quan. Spectros. Radiat. Trans.* **1975**, *11*, 45.

(22) Hönl-London factors for 3Σ−3Σ transition were calculated according to formulas. Tatum, J. B. *Can. J. Phys.* **1966**, *44*, 2944.

(23) Okabe, H. *Photodissociation of Small Molecules*; John Wiley & Sons: New York, 1978.

3.2. Time Dependent Production of SO($X^3\Sigma^-$). In addition to the direct photolytic production of SO($X^3\Sigma^-$), we also have observed a second time-dependent growth channel for ground-state sulfur monoxide. We have characterized this process by recording temporal profiles of the total SO($X^3\Sigma^-$) production. In these measurements, the probe laser was fixed at a wavelength corresponding to a rovibronic transition of the SO fragment, and the delay time between the photolysis and probe laser was varied from 0 to 300 μs. We found that the LIF intensity of the SO($X^3\Sigma^-$, $v'' = 0-6$) fragment initially increased with increasing delay time between the pump and probe lasers and then decayed. The LIF signal intensity reaches its maximum at a delay time of *ca*. 50−100 μs (*i.e*., 100−200 collisions). The time dependence of the LIF signal of the SO($X^3\Sigma^-$, $v'' = 1$) photofragment following 248 nm photolysis is shown in Figure 3. The magnitude of the relative rate of growth of the LIF signal increases with increasing vibrational level for $v'' = 1-6$.

One possibility for the origin of this time dependent increase in SO($X^3\Sigma^-$) may be due to the relaxation of the excited states of SO, *i.e*., those that were initially produced in the photolysis of C_2H_4SO. Direct infrared spectroscopic studies by Kanamori *et al*. show that the decay of SO($a^1\Delta$) state under similar conditions is comparable in time to our growth curve.[24] By using a kinetic analysis, we can obtain the analytical expression of the SO($X^3\Sigma^-$) concentration as a function of time, which can be used to fit the experimental data. $C_2H_4SO^*$ is the photoactived ethylene episulfoxide, which decomposes to produce SO and other products. [SO(X)] and [SO(a)] are the concentrations of SO in the ($X^3\Sigma^-$) and ($a^1\Delta$) electronic states, respectively.

The kinetic processes to be considered in our analysis are

$$C_2H_4SO^* \xrightarrow{k_1} SO(X) + C_2H_4 \quad (3)$$

$$C_2H_4SO^* \xrightarrow{k_2} SO(a) + C_2H_4 \quad (4)$$

$$C_2H_4SO^* \xrightarrow{k_3} \text{other products} \quad (5)$$

$$SO(a) + M \xrightarrow{k_r} SO(X) + M \quad (6)$$

$$SO(X) + M \xrightarrow{k_D} \text{secondary reactions and diffusion} \quad (7)$$

$$SO(a) + M \xrightarrow{k'_D} \text{secondary reactions and diffusion} \quad (8)$$

When the total pressure is low, $k = k_1 + k_2 + k_3 \gg k_r[M]$ and $k_D[M]$, and assuming that all the SO molecules in ($a^1\Delta$) state are relaxed to the ground state, *i.e*., $k'_D \approx k_r$, the time dependent solution for the concentration of SO($X^3\Sigma^-$) becomes[25]

$$[SO(X)] = \frac{[C_2H_4SO]_0^*}{k}\left\{k_1(e^{-k_D[M]t} - e^{-kt}) + \frac{k_r}{k_r - k_D}k_2(e^{-k_D[M]t} - e^{-k_r[M]t})\right\} \quad (9)$$

Since the LIF signal is proportional to the concentration of SO(X), we use the following eq to fit the experimental data

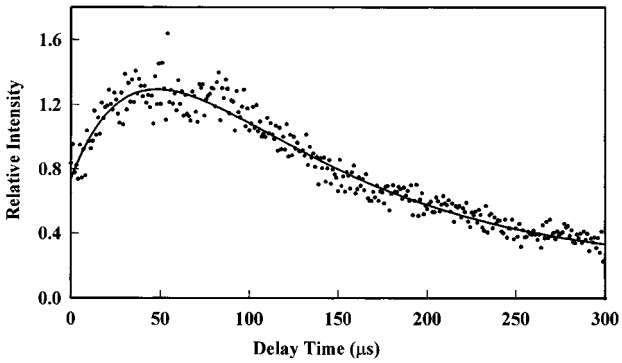

Figure 3. LIF transient signal of the SO($B^3\Sigma^-$,$v' = 1$ − $X^3\Sigma^-$ $v'' = 1$) transition following 248 nm photolysis of C_2H_4SO. The solid curve is the best fit to the experimental data using eq 10.

Table 2. The Branching Ratios and Quantum Yields of SO($X^3\Sigma^-$) and SO($a^1\Delta$)

photolysis wavelength (nm)	branching ratio R	quantum yield of SO($X^3\Sigma^-$)	quantum yield of SO($a^1\Delta$)	total quantum yield of SO
193	1.65	0.25 ± 0.04	0.41 ± 0.06	0.66 ± 0.10
248	1.28	0.34 ± 0.06	0.44 ± 0.08	0.78 ± 0.14

$$[SO(X)] = A(e^{-k_D[M]t} - e^{-kt}) + B(e^{-k_D[M]t} - e^{-k_r[M]t}) + C \quad (10)$$

where A, B, $k_D[M]$ and $k_r[M]$ are parameters. The arbitrary constant, C, accounts for the LIF background signal. The branching ratio (*cf*. eqs 3 and 4) of [SO(a)] to [SO(X)] is k_2/k_1. Comparison of eqs 9 and 10 yield the branching ratio, R

$$R = \frac{k_2}{k_1} = \frac{B}{A}\frac{k_r[M] - k_D[M]}{k_r[M]} \quad (11)$$

Since 50−65% of the nascent SO($X^3\Sigma^-$) fragments populate the first excited vibrational level, we report the best fit values of the observed time dependence of the LIF signal of SO($X^3\Sigma^-$) due to $v'' = 1$. Similar fits can be obtained for different vibrational levels, but the results are qualitatively the same. We assume that the decomposition processes 3−5 are fast, *i.e*., they are completed within 200 ns, resulting in $k = 5.0\ \mu s^{-1}$. A typical fit to the experimental data is shown in Figure 3. From these fits, we find that the branching ratios are 1.65 and 1.28 for 193 and 248 nm photolyses, respectively. In the context of this kinetic model and the assumptions made, the quantum yield of the nascent SO($a^1\Delta$) fragment and the total SO quantum yield can then be estimated based on the branching ratio and the observed quantum yield of SO($X^3\Sigma^-$). The results are summarized in Table 2.

4. Discussion

Our results demonstrate that C_2H_4SO undergoes photoelimination of the SO radical following 193 and 248 nm irradiation. One of the attractive ideas about studying the photochemistry of ethylene episulfoxide is the possibility of determining a convenient source of the first electronic excited state of SO radical, *i.e*., $^1\Delta$ state, which lies about 18 kcal/mol above the ground state.[26] To date, the only direct measurement of an SO($a^1\Delta$) photofragment has been from the 193 nm photodissociation of thionyl chloride.[27,28] Our experimental results show that the LIF signal of the SO($X^3\Sigma^-$) photofragment following

(24) Kanamori, H.; Tiemann, E.; and Hirota, E. *J. Chem. Phys*. **1988**, *89*, 621.

(25) For a full derivation of this equation, see: Wu, F., Ph.D. Dissertation, University of Puerto Rico, 1996, pp 58−60.

(26) Huber, K. P.; Herzberg, G. *Molecular Spectra and Molecular Structure*; Van Nostrand Reinhold Company: New York, 1979; Vol. IV.

(27) Kanamori, H.; Hirota, E. *J. Chem. Phys*. **1988,** *89*, 621.

photolysis of ethylene episulfoxide grows with increasing delay time between the two lasers. The maximum intensity was obtained after *ca.* 100−200 collisions. The origin of this increase in LIF intensity is most likely due to the relaxation of the excited SO($a^1\Delta$) fragment. Thus, there are two channels to produce the SO($X^3\Sigma^-$) photofragment at both photolysis wavelengths. One channel is a fast process which produces SO($X^3\Sigma^-$) directly from the decomposition of the excited C_2H_4-SO molecule. The second channel is a slow process producing the SO($X^3\Sigma^-$) fragment from the relaxation of the electronically excited SO. The relaxation may be due to a quenching process as shown in eq 6, phosphorescence (which may be probed directly by measuring the infrared emission signal near 1.6 μm), or a combination of the two. If we assume that there are only two SO production channels, *i.e.*, reactions 3 and 4, which can occur following ultraviolet irradiation of C_2H_4SO, we can carry out a kinetic analysis to calculate the time behavior of the LIF signal of SO($X^3\Sigma^-$) photofragment as shown in the previous section. We neglect the small diffusion and other bimolecular reactions with the SO($a^1\Delta$) fragment and assume that most of the excited state undergoes relaxation to the ground state. By fitting eq 10 to the experimental data, we have estimated the branching ratio for the two SO production channels (*cf.* Table 2). Based on the observed quantum yields of the nascent SO($X^3\Sigma^-$) photofragments produced in reaction 3 and the branching ratios, the quantum yields of the SO($a^1\Delta$) photofragment were estimated to be 0.41 ± 0.06 and 0.44 ± 0.08 for 193 and 248 nm photolyses, respectively. The total quantum yields of SO production, including ground-state SO($X^3\Sigma^-$) and excited state SO($a^1\Delta$), are 0.66 ± 0.10 and 0.78 ± 0.14 following 193 and 248 nm photolysis of C_2H_4SO.

The nascent vibrational state distributions of the SO($X^3\Sigma^-$) photofragment in the direct production channel following both 193 and 248 nm irradiation are inverted with maximum populations at $v'' = 1$. This suggests that the photodissociation of C_2H_4SO, at both 193 and 248 nm, proceeds via a concerted bond cleavage process in which the two C−S bonds break faster than energy redistribution to yield an SO photofragment. Inverted vibrational state distributions of the SO($X^3\Sigma^-$) photofragment have been found previously in our laboratory following the UV photolysis of $(CH_3)_2SO$, F_2SO, Cl_2SO, and Br_2SO.[17] All the inverted vibrational state distributions of SO($X^3\Sigma^-$) photofragment have been attributed to a concerted bond cleavage mechanism. A statistical vibrational state distribution might be expected if the photodissociation proceeded via a stepwise process.[8]

In order to obtain more insight into the dissociation mechanism, we have (1) constructed a state correlation diagram (see Figure 4) based on an interaction model suggested by Hoffmann *et al.*,[29] (2) modeled the nascent vibrational state distributions with a Franck−Condon physical model, and (3) analyzed the energy partitioning into the internal degrees of freedom of the SO($X^3\Sigma^-$) fragment in conjunction with an impulsive model, which has been generalized to apply to the photofragmentation of cyclic compounds.

In studying the irregular trends in the bond distances in going from ethylene episulfide to ethylene episulfoxide to ethylene episulfone, Hoffmann and co-workers suggested a bonding picture in which these three heterocyclic molecules are described as complexes of an ethylene with S, SO, and SO_2, respectively.[29] For ethylene episulfoxide, the bonding mechanism was described in terms of a donor−acceptor complex between ethylene and sulfur monoxide. The π orbital of ethylene (donor) and the empty π^* orbital of SO (acceptor) are symmetric with respect to the plane perpendicular to the C−C bond which also contains the S−O bond in ethylene episulfoxide. Interaction of these two symmetric orbitals of the ethylene and SO fragments yields a bonding molecular orbital *S* and an anti-bonding molecular orbital *S** in ethylene episulfoxide. There is also a reverse electron donation from the occupied π^* orbital of the SO fragment to the π^* orbital of the ethylene fragment. These two orbitals are antisymmetric and form a bonding molecular orbital *A* and an anti-bonding molecular orbital *A**. Four electrons populate the *S* and *A* orbitals stabilizing the complex. Since the four molecular orbitals *S*, *A*, *S**, and *A** are responsible for the bonding between the ethylene and SO fragments in this framework, the transition of an electron from one of the bonding orbitals, *S* and *A*, to one of the antibonding orbitals, *S** and *A**, would be directly responsible for the dissociation of ethylene episulfoxide into the SO and C_2H_4 fragments. The four molecular orbitals have a clear correlation with the π and/or π^* orbitals of the ethylene and SO fragments, allowing us to construct a state correlation diagram between reactant (C_2H_4-SO) and products (C_2H_4 + SO) by moving one electron from bonding orbitals *S* and *A* to the anti-bonding orbitals *S** and *A** with all possible spin orientations. The resulting state correlation diagram is shown in Figure 4. The reactant excited states in this diagram are those that may be responsible for the dissociation of C_2H_4SO into SO and C_2H_4 products. Due to the ring strain and the relatively weak C−S bond, the dissociation of ethylene episulfoxide into SO and an ethylene fragment may be easier than any other fragmentation channel. The relative ordering of the reactant states of the same multiplicity is obtained directly from the ordering of the four molecular orbitals.[29] The relative ordering between triplet and singlet states can not be obtained directly from the ordering of the molecular orbitals because the spin−spin and spin−orbital couplings are not known. A single point *ab initio* calculation of C_2H_4SO using the ground-state geometry, has been carried out by using the Gaussian 92 program package at the CIS (configuration interaction with single substitutions) level with a 6-31G* basis set.[30] The calculated results indicated that there are four triplet excited states that are lower in energy than the first excited singlet state. Although the absolute energies of the excited states from this calculation are dubious, the relative ordering between the triplet

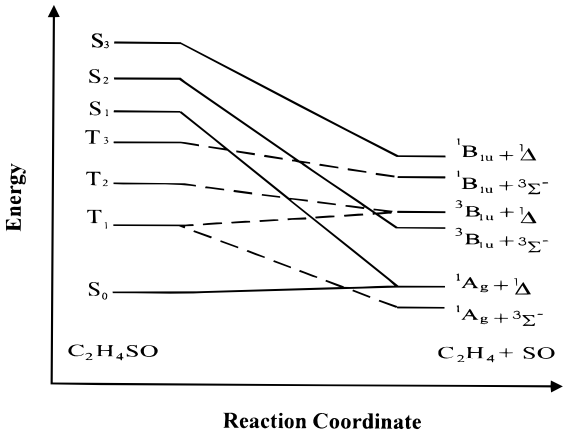

Figure 4. State correlation diagram for the photolysis of C_2H_4SO to yield the products and C_2H_4 + SO.

(28) Endo, Y.; Kanamori, H.; Hirota, E. *Chem. Phys. Lett.* **1987**, *141*, 129.

(29) Hoffmann, R.; Fujimoto, H.; Swenson, J. R.; Wan, C. *J. Am. Chem. Soc.* **1973**, *95*, 7644.

(30) Gaussian 92, Revision G.3; Frish, M. J.; Trucks, G. W.; Head-Gordon, M.; Gill, P. M. W.; Wong, M. W.; Foresman, J. B.; Johnson, B. G.; Schlegel, R. M. A.; Replogle, E. S.; Gomperts, R.; Andres, J. L.; Raghavachari, K.; Binkley, J. S.; Gonzalez, C.; Martin, R. L.; Fox, D. J.; Defrees, D. J.; Baker, J.; Stewart, J. J. P.; Pople, J. A. Gaussian, Inc.: Pittsburgh, PA, 1992.

Table 3. Franck−Condon/Golden Rule Best Fit Parameters for the Photodissociation of Ethylene Episulfoxide

photolysis wavelength	193 nm	248 nm
bond length	1.495 Å	1.532 Å
bond strength	1100 cm^{-1}	1100 cm^{-1}
available energy	67 kcal/mol	35 kcal/mol

and singlet states is clearly seen. Based on this result, we assume that all three triplet states, *i.e.*, T_1, T_2, and T_3, in the correlation diagram of Figure 4 are lower in energy than the first excited singlet state S_1. The energy ordering of the products' states is obtained from the experimental data.[26,31] The resulting correlation diagram is used to help elucidate a clear dissociation mechanism (*vide infra*).

The experimental vibrational state distributions can be compared with those calculated on the basis of a Franck−Condon physical model. A Franck−Condon/Golden Rule treatment has been used previously to model inverted vibrational state distributions of nascent products from elementary reactions.[17a,b,32] This model assumes a sudden transition from a "dressed" oscillator, *e.g.*, SO in the parent polyatomic molecule, to the "undressed" diatomic photofragment, $SO(X^3\Sigma^-)$, and calculates the probability, $P(f)$, of its formation in vibrational state, $|f\rangle$

$$P(f) \propto (4\pi^2/h)|\langle i|f\rangle|^2\rho(E) \qquad (12)$$

where $|i\rangle$ is the initial " dressed oscillator " state, corresponding to SO in the parent molecule, *e.g.*, SO in ethylene episulfoxide. ρ(E) is the density of final states at available energy, E, and h is Planck's constant. Morse oscillator wave functions are used for $|f\rangle$ and $|i\rangle$. To the extent that this model is a valid portrayal of the dissociation event, application of eq 12 to the photofragmentation of ethylene episulfoxide reveals the bond length of the "dressed" S═O moiety immediately prior to fragmentation. Best fits of the calculated vibrational state distributions to the experimental data are shown in Figure 1 and are summarized in Table 3.

The above bond lengths, resulting from the Franck−Condon model, were obtained by using the available energies corresponding to the formation of $SO(X^3\Sigma^-)$ in concert with a triplet ethylene

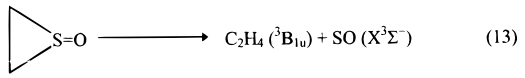

(13)

If we use the available energies corresponding to the formation of ground-state ethylene, then the Franck−Condon model cannot adequately fit the experimental data. Within the context of this model, this reveals that the $SO(X^3\Sigma^-)$ photofragment is decoupled from the hydrocarbon skeleton before the stable final products are formed.

To further illustrate the concerted nature of this dissociation, we have generalized an impulsive model to apply to the photofragmentation of cyclic compounds. This impulsive model, developed by Busch and Wilson, was used to model the direct dissociations of triatomic molecules, $\alpha\beta\gamma$, using the classical formulation based on momentum transfer.[33] When the

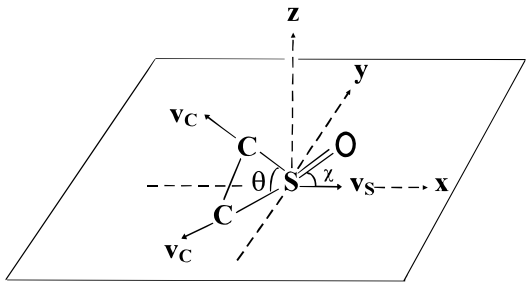

Figure 5. The geometry of ethylene episulfoxide used in the application of the impulsive model.

$\alpha-\beta$ bond dissociates, it is assumed that the atoms α and β recoil sharply and release the energy before the atom γ has time to respond. The available energy (E_{avl}) is partitioned by conservation of linear momentum between the kinetic energies of α and β in the inverse ratio of their masses. The recoiling atom β is still bonded to γ, and the initial kinetic energy of the atom (β) is now distributed among translational, rotational, and vibrational degrees of freedom of the diatomic fragment $\beta\gamma$. According to this model, the total translational energy of both fragments, E_T, is related to the available energy E_{avl} by

$$E_T = (\mu_\alpha/\mu_f)E_{avl} \qquad (14)$$

where μ_α is the reduced mass of the two atoms α and β, at the ends of the breaking bond, and μ_f is the reduced mass of the fragments, α and $\beta\gamma$. By conservation of energy, the energy partitioned into the internal degrees of freedom (rotation and vibration) of the $\beta\gamma$ fragment is

$$E_{V+R}(\beta\gamma) = (1 - \mu_\alpha/\mu_f)E_{avl} \qquad (15)$$

Houston and co-workers have generalized this model to apply to polyatomic molecules.[34] They considered the dissociation of polyatomic molecule AB into fragments A and B, each of which may also be polyatomic. This generalized model was applied to the photodissociation of acetone at 193 nm to fit the energy partitioning between the fragments.[34]

We have further developed this impulsive model to apply it to the dissociation of cyclic compounds in which two bonds break in a concerted manner to produce a diatomic fragment and other polyatomic fragments. In this case, the detailed geometry of the dissociating molecule must be considered. To clearly illustrate this model, consider the ethylene episulfoxide example shown in Figure 5, where m_C, m_S, and m_O are the atomic masses of carbon, sulfur, and oxygen, respectively. If we assume that this ring compound dissociates in a concerted manner, *i.e.*, the two C−S bonds break simultaneously, then, at the moment of the fragmentation, the sulfur atom and the two carbon atoms gain their initial kinetic energies with initial velocities v_S and v_C, respectively. By conservation of energy, the total available energy E_{avl} can be represented by

$$E_{avl} = 2 \times \frac{1}{2}m_C v_C^2 + \frac{1}{2}m_S v_S^2 \qquad (16)$$

Since the two dissociative coordinates are identical, the impulse along the two bonds should be the same. The direction of the recoil velocity of the sulfur atom must be along the bisection of the C−S−C angle, *i.e.*, the x direction in Figure 5. By conservation of linear momentum in the x direction, we have

(31) Herzberg, G. *Molecular Spectra and Molecular Structure III. Electronic Spectra and Electronic Structure of Polyatomic Molecules*. Krieger Publishing Company: Florida, 1991; p 629.

(32) (a) Berry, M. J., *Chem. Phys. Lett.* **1974**, *29*, 323,329. (b) Chen, X.; Asmar, F.; Wang, H.; Weiner, B. R., *J. Phys. Chem.* **1991**, *95*, 756. (c) Berry, M. J.; *J. Chem. Phys.* **1974**, *39*, 3114. (d) Schatz, G. C.; Ross, J., *J. Chem. Phys.* **1977**, *66*, 1037. (e) Mukamel, S.; Jortner, J.; *J. Chem. Phys.* **1974**, *60*, 4760.

(33) Busch, G. E.; Wilson, K. R. *J. Chem. Phys.* **1972**, *56*, 3626.

(34) Trentelman, K. A.; Kable, S. H.; Moss, D. B.; Houston, P. L. *J. Chem. Phys.* **1989**, *91*, 7498.

$$2m_C v_C \cos\frac{\theta}{2} = -m_S v_S \quad (17)$$

where θ is the C−S−C bond angle. The total energy partitioned into the SO fragment, E(SO), is equal to the initial kinetic energy of the sulfur atom.

$$E(\mathrm{SO}) = \frac{1}{2} m_S {v_S}^2 \quad (18)$$

From eqs 16−18, the energy content (total, translational, vibrational, and rotational) of the SO fragment can be related to the available energy by

$$E(\mathrm{SO}) = \frac{2m_C \cos^2\frac{\theta}{2}}{m_S + 2m_C \cos^2\frac{\theta}{2}} E_{avl} \quad (19)$$

By conservation of momentum, the translational energy of the SO fragment is

$$E_T(\mathrm{SO}) = \frac{m_S}{m_S + m_O} E(\mathrm{SO}) \quad (20)$$

The total internal (vibrational and rotational) energy of the SO fragment, by conservation of energy, is

$$E_{V+R}(\mathrm{SO}) = \left(1 - \frac{m_S}{m_S + m_O}\right) E(\mathrm{SO}) \quad (21)$$

Substituting (19) into (21), we have

$$E_{V+R}(\mathrm{SO}) = \left(1 - \frac{m_S}{m_S + m_O}\right) \frac{2m_C \cos^2\frac{\theta}{2}}{m_S + 2m_C \cos^2\frac{\theta}{2}} E_{avl} \quad (22)$$

If the angle between the S-O bond and the C−S−C plane is χ, then the energies partitioned into the vibrational and rotational degrees of freedom of the SO fragment, by analogy to the triatomic system, are represented by

$$E_V = E_{V+R} \cos^2\chi \quad (23)$$

$$E_R = E_{V+R} \sin^2\chi \quad (24)$$

We assume that the bond angle θ in the transition state, immediately prior to the two bonds breaking, is similar to the corresponding angle in the ground state. By using the experimental value of $\theta = 48° 46'$, obtained by microwave spectroscopy,[35,36] we can calculate the percentage of the available energy partitioned into the internal degrees of freedom of the SO fragment, $E_{V+R}/E_{avl} = 12.8\%$. To compare the calculated results with our experimental observation, the energy disposal into the SO fragment was analyzed. The energy disposal into the vibrational degree of freedom of the SO($X^3\Sigma^-$) fragment was evaluated as the sum of the energy partitioned into each vibrational level: $E_{vib} = \sum c_{v''}(E(v'') - E_0)$, where $c_{v''}$ is the fractional population in v'' state obtained from Figure 1a,b, for the 193 and 248 nm photolyses, respectively. $E(v'')$ and E_0 are the energies of the given vibrational level, v'', and the zero point energy of the electronic state, respectively. The average rotational energy, E_{rot}, for the SO($X^3\Sigma^-$) fragment was estimated by $\sum c_{v''}(k_B T_{rot}(v''))/\sum c_{v''}$, where $T_{rot}(v'')$ is the rotational temperature in the given vibrational state, k_B is the Boltzmann constant, and other variables are the same as given above. We have used the available energy listed in Table 3, corresponding to the reaction of eq 13, to evaluate the percentage of the available energy channeled into the internal degrees of freedom of the SO($X^3\Sigma^-$) fragment. The results are summarized in Table 4.

Table 4. Energy Disposal into the Internal Degrees of Freedom of the Nascent SO($X^3\Sigma^-$) Photofragment Following 193 and 248 nm Photolyses of Ethylene Episulfoxide

wavelength (nm)	experimental (%)			impulsive model	
	E_V/E_{avl}	E_R/E_{avl}	E_{V+R}/E_{avl}	E_{V+R}/E_{avl} (%)	χ (deg)
193	7.7	2.6	10.3	12.8	30.2
248	9.6	3.8	13.8	12.8	33.5

Table 4 shows that the observed energy partitioning into the internal degrees of freedom of the SO($X^3\Sigma^-$) fragment agrees well with that calculated by the impulsive model for both photolysis wavelengths, provided that we use the available energy corresponding to the production of the $C_2H_4(^3B_{1u})$ and SO($X^3\Sigma^-$) fragments. This result is consistent with a concerted fragmentation process to produce ethylene in the $^3B_{1u}$ state and SO in the ground electronic state. By using eqs 23 and 24 as well as the observed values of E_V and E_R, we estimate the angle, χ, between the SO bond and the plane containing the two C−S bonds (see Figure 5). The estimated values of χ for 193 and 248 nm photolyses are listed in Table 4. In the ground state of ethylene episulfoxide, the angle χ is about 66°. The estimated values of χ based on the observed energy partitioning for both photolysis wavelengths are smaller than that in the ground state.

Our results show that the direct photoproduction of SO($X^3\Sigma^-$) from C_2H_4SO appears to be undergoing a similar mechanism following irradiation at either 193 or 248 nm. Both photodissociation wavelengths produce inverted vibrational distributions with maxima at $v'' = 1$ and similar trends in rotational state distributions in nascent SO($X^3\Sigma^-$) product. The branching ratios for the production of SO($X^3\Sigma^-$) and SO($a^1\Delta$) are also similar. In the 193 nm case, the best fit bond lengths are similar to those of the ground state of the corresponding episulfoxide.[36,37] One possibility, consistent with the state correlation diagram, is that ethylene episulfoxide undergoes direct dissociation from an S_2 repulsive potential energy surface to produce SO in $B^3\Sigma^-$ state and ethylene in $^3B_{1u}$ state, following 193 nm irradiation. Production of the SO($a^1\Delta$) photofragment would then occur on the S_1 surface following rapid internal conversion. A similar explanation can also be applied to the 248 nm photolysis mechanism. The UV absorption spectrum of ethylene episulfoxide is structureless with an onset around 250 nm indicating that there may be a strong mixing of S_1 and S_2 states. Our single point *ab initio* CIS calculations to determine excited state energies of the parent molecule, also indicate that S_2 is the only state to carry any significant oscillator strength. The SO fragments are produced on the same surfaces at both photolysis wavelengths, *i.e.*, SO($X^3\Sigma^-$) produced on the S_2 surface and SO($a^1\Delta$) produced on the S_1 surface. The rotational temperatures of the SO($X^3\Sigma^-$) photofragments at different vibrational levels show the same trends for 193 and 248 nm photolysis. These results suggest that the SO($X^3\Sigma^-$) photofragment is produced on the same surface following 193 and 248 nm photolysis.

(35) White, W. F.; Wollrab, J. E. *Chem. Phys. Lett.* **1969**, *3*, 15.
(36) Saito, S. *Bull. Chem. Soc. Jpn.* **1969**, *42*, 663.
(37) Bevan, J. W,; Legon, A. C.; Millen, D. J. *Proc. Roy. Soc. (London)* **1977**, *A354*, 491.

5. Summary and Conclusions

We have reported here the first studies of the ultraviolet photochemistry of the ethylene episulfoxide. Our results and analysis can be summarized as follows:

1. The nascent $SO(X^3\Sigma^-)$ vibrational state distributions following 193 and 248 nm photolyses of C_2H_4SO show significant excitation in the diatomic photofragment (up to $v'' = 6$), and are both inverted with maxima at $v'' = 1$. The nonstatistical nature of the vibrational state distributions strongly indicate that the $SO(X^3\Sigma^-)$ is produced by concerted cleavage of the two C−S bonds.

2. Two physical models, Franck−Condon and impulsive, have been used to model the distribution of internal energy in the $SO(X^3\Sigma^-)$ photofragment. Both models demonstrate that a reasonable fit to the experimental data is obtained only when the other product of the photolysis is $C_2H_4(^3B_{1u})$ and not ground-state ethylene. The models also yield information about the transition state geometries of the photoreaction, revealing no significant difference between 193 and 248 nm photolysis.

3. A second, time-dependent $SO(X^3\Sigma^-)$ production channel has been identified and assigned to the relaxation of $SO(a^1\Delta)$, produced in the photolysis. On the basis of the detailed kinetic analysis, branching ratios, $SO(a^1\Delta)/SO(X^3\Sigma^-)$, of 1.65 and 1.28 have been measured for the 193 and 248 nm photolyses, respectively. By comparison with SO_2 photolysis, absolute quantum yields for the processes have been determined.

4. Construction of a state correlation diagram has allowed us to show that both 193 and 248 nm photolyses proceed via a S_2 excited state to produce $SO(X^3\Sigma^-)$ in concert with $C_2H_4(^3B_{1u})$. The $SO(a^1\Delta)$ is believed to originate from an S_1 excited state which results following rapid internal conversion from S_2.

Acknowledgment. These experiments were performed in the Puerto Rico Laser and Spectroscopy Facility at the University of Puerto Rico, which has been developed through the generosity of the NSF-EPSCoR and NIH-RCMI programs. The support of the Air Force Office of Scientific Research, through Grants F4962-92-5-0406 and F49620-93-1-0110, is gratefully acknowledged. F.W. thanks the UPR Materials Research Center for its support. The authors kindly acknowledge Dr. John Lombardi and Dr. K. Ravichandran for helpful discussions and thank Dr. Edgar Miranda Avalo, Dr. Anil Rane and Mr. Karl Matos Pizarro for their help in the synthesis of the title compound.

JA960968O